ЖЭТФ, 2004, том 125, вып. 6, стр. 1423–1435

JOSEPHSON CHARGE-PHASE QUBIT WITH THE RADIO FREQUENCY READOUT: COUPLING AND DECOHERENCE

A. B. Zorin*

Physikalisch-Technische Bundesanstalt
38116, Braunschweig, Germany

Institute for Nuclear Physics, Moscow State University
119899, Moscow, Russia

Submitted 10 December 2003

The Josephson qubit based on a superconducting single charge transistor inserted in a low-inductance superconducting loop is considered. The loop is inductively coupled to a radio-frequency driven tank circuit enabling the readout of the qubit states by measuring the effective Josephson inductance of the transistor. The effect of qubit dephasing and relaxation due to electric and magnetic control lines as well as the measuring system is evaluated. Recommendations for the qubit operation with minimum decoherence are given.

PACS: 74.50.+r, 85.25.Cp, 03.67.Lx

1. INTRODUCTION

The superconducting quantum bit (qubit) circuits comprising mesoscopic Josephson tunnel junctions have recently demonstrated remarkable quantum coherence properties and are now considered promising elements for a scalable quantum computer [1]. But the readout of macroscopic quantum states of a single qubit or a system of coupled qubits with the minimum decoherence caused by the detector remains one of the most important engineering issues in this field.

The Josephson qubits are commonly subdivided into flux, phase, charge and charge-phase qubits. The design of charge and charge-phase qubits is based on a Cooper pair box [2] in which a small superconducting island with significant Coulomb energy is charged through a small Josephson junction (charge qubit) or a miniature double-junction SQUID (charge-phase). The distinct quantum states of the box generated by signals applied to a gate are associated with different observable charges on the island. This makes it possible to read out the qubit state by discriminating the island charge. Probing this charge can be done either by single quasiparticle tunneling across a small auxiliary tunnel junction attached to the island [3] or by a capacitively coupled electrometer [4]. In the charge-phase qubits, the quantum states of the box involve the phase coordinate of the SQUID loop, and hence discriminating these states can also be done by measuring the persistent current circulating in the loop at an appropriate dc flux bias. Such a measurement was performed in the experiment of the Saclay group [5]. In their setup, nicknamed «Quantronium», the circulating current passed through a larger auxiliary (third) junction was read out by measuring the switching current of this junction.

The persistent current is not the only phase-dependent quantity characterizing the quantum state of the charge-phase qubit. Another useful quantity is the Josephson inductance of the double junction, which can be probed by small radio-frequency oscillations induced in the qubit. Recently, we proposed a transistor configuration of the Cooper pair box (see Fig. 1) in which the macroscopic superconducting loop closing the transistor terminals is inductively coupled to a radio-frequency tank circuit [6]. Similar to the rf-SQUID-based method of measurement of the Josephson junction impedance [7], this setup makes it possible to measure the rf impedance (more specifically, the Josephson inductance) of the system of two small tunnel junctions connected in series, and in doing so, to probe the macroscopic states of the qubit.

On one hand, the advantage of this method consists in an effective decoupling between the qubit and a

*E-mail: alexander.zorin@ptb.de

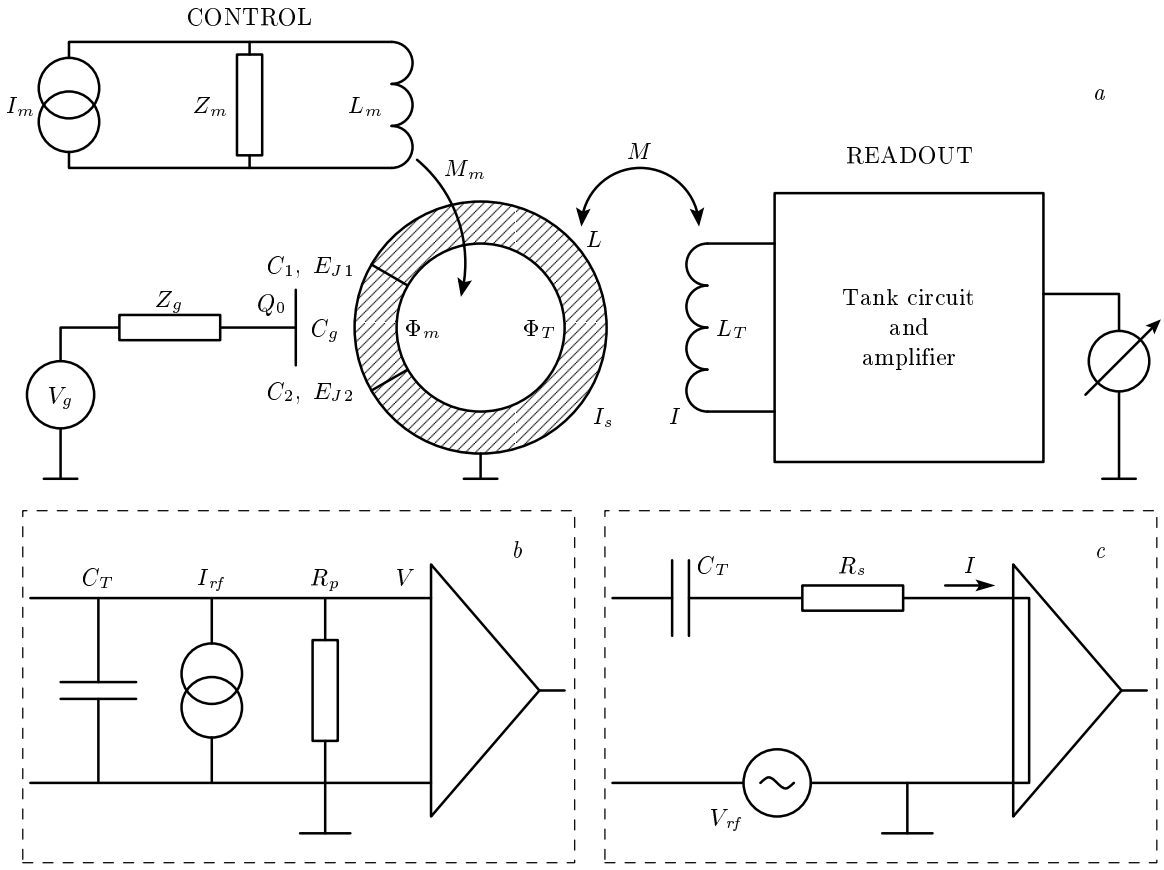

Fig. 1. *a*) The electric circuit diagram of the charge-flux qubit inductively coupled to a tank circuit by the mutual inductance M. The macroscopic superconducting loop of inductance L is interrupted by two small Josephson tunnel junctions positioned close to each other and forming a single-charge transistor; the capacitively coupled gate polarizes the island of this transistor. The qubit is controlled by the charge Q_0 generated by the gate and the flux Φ_m induced by coil L_m. The tank circuit, which is either of a parallel (*b*) or a serial (*c*) type, is driven by a harmonic signal (I_{rf} or V_{rf}, respectively) of the frequency $\omega_{rf} \approx \omega_0$, the resonant frequency of the uncoupled tank circuit

measurement device, which reduces the decoherence of the qubit. Moreover, the loop design of the qubit has a potential to perform data readout in a nondestructive way [8]. On the other hand, due to the selective characteristic of the tank, the bandwidth of this setup is rather narrow, and therefore the optimum relation between the relaxation time of the qubit and the time of measurement becomes an issue. Furthermore, the driving rf signal may induce appreciable frequency modulation and dephasing of the qubit during its evolution (performance of the quantum operations). Switching the oscillations off and on is, however, possible only on a relatively long-time scale of a transient process in the tank.

In this paper, we address the problem of decoherence induced in the charge-flux qubit by the classical resonance tank circuit. In addition, we propose a measurement strategy and optimize the regime of qubit operation for typical parameters of the circuit.

2. BACKGROUND

The small tunnel junctions of the charge-flux qubit are characterized by self-capacitances C_1 and C_2 and the Josephson coupling strengths E_{J1} and E_{J2}. These junctions with a small central island in-between and a capacitively coupled gate therefore form a single-charge transistor connected in our network as the Cooper pair box (see Fig. 1). The critical currents of the junctions are equal to

$$I_{c1,c2} = \frac{2\pi}{\Phi_0} E_{J1,J2},$$

where $\Phi_0 = h/2e$ is the flux quantum, and their mean value is

$$I_{c0} = \frac{1}{2}(I_{c1} + I_{c2}).$$

The design enables magnetic control of the Josephson coupling in the box in a dc SQUID manner. The system therefore has two parameters, the total Josephson phase across the two junctions $\phi = \varphi_1 + \varphi_2 = 2\pi\Phi/\Phi_0$ controlled by the flux Φ threading the loop and the gate charge Q_0 set by the gate voltage V_g. The geometrical inductance L of the loop is assumed to be much smaller than the Josephson inductance of the junctions $L_{J0} = \Phi_0/(2\pi I_{c0})$,

$$\beta_L = L/L_{J0} \ll 1. \tag{1}$$

Neglecting the magnetic energy term associated with the current through the small inductance L, we can express the Hamiltonian of the autonomous qubit circuit as

$$H_0 = \frac{(2en - Q_0)^2}{2C} - E_J(\phi)\cos\chi. \tag{2}$$

The second term in Eq. (2) originates from the total Josephson energy equal to $-E_{J1}\cos\varphi_1 - E_{J2}\cos\varphi_2$. The effective Josephson coupling strength is

$$E_J(\phi) = \left(E_{J1}^2 + E_{J2}^2 + 2E_{J1}E_{J2}\cos\phi\right)^{1/2}, \tag{3}$$

$$|E_{J1} - E_{J2}| \le E_J(\phi) \le E_{J1} + E_{J2} \equiv 2E_{J0} = \frac{\Phi_0}{\pi} I_{c0},$$

with the phase variable $\chi = \varphi + \gamma(\phi)$. The angle γ is given by

$$\operatorname{tg}\gamma = (j_1 - j_2)\operatorname{tg}(\phi/2), \tag{4}$$

where the dimensionless Josephson energies are $j_{1,2} = E_{J1,J2}/(2E_{J0})$ with $j_1 + j_2 = 1$. The phase difference $\varphi = \frac{1}{2}(\varphi_1 - \varphi_2)$ is a variable conjugate to the island charge $2en = -2ei\frac{\partial}{\partial\varphi}$ and n is the operator of the number of excess Cooper pairs on the island. This charge enters the charging energy (first) term in Eq. (2), in which C is the total capacitance of the island, $C = C_1 + C_2 + C_g \approx C_1 + C_2$, and the gate capacitance $C_g \ll C_{1,2}$. The characteristic charging energy $E_c = e^2/2C$ is assumed to be of the order of the Josephson coupling energies $E_{J1} \sim E_{J2} \gg k_B T$.

The Schrödinger equation corresponding to the Hamiltonian in Eq. (2) is the Mathieu equation [9]. The eigenenergies form Bloch bands and the eigenfunctions $|n, q\rangle$ are the Bloch wave functions of a particle in the periodic (Josephson) potential with «quasimomentum» (here, quasicharge) q. Its value is the charge provided by the gate source to the island, i.e., $q = Q_0 = C_g V_g$. Each of such eigenfunctions can be represented as a coherent superposition of plane waves,

$$|q, n\rangle = \sum_m C_m^{(n)} \exp\left[i\left(\frac{q}{2e} + m\right)\chi\right], \tag{5}$$

where $m = 0, \pm1, \pm2, \ldots$ is the number of the excess Cooper pairs on the island [10, 11]. The weights of these coherent contributions $|C_m^{(n)}|^2$ depend on q, the band index n, and the characteristic ratio

$$\lambda = E_J(\phi)/E_c. \tag{6}$$

The lowest two energy levels $E_n(q, \phi)$, i.e., $n = 0$ and 1 (see their dependences on q and ϕ in Fig. 2) form the basis $\{|0\rangle, |1\rangle\}$ suitable for qubit operation. In this basis, Hamiltonian (2) is diagonal,

$$H_0 = -\frac{1}{2}\epsilon\sigma_z, \tag{7}$$

where σ_i with $i = x, y, z$ is the Pauli spin operator. The general state of the qubit is

$$|\Psi\rangle = a|0\rangle + b|1\rangle, \tag{8}$$

with $|a|^2 + |b|^2 = 1$. It is remarkable that the level spacing $\epsilon(q, \phi) \equiv \hbar\Omega = E_1(q, \phi) - E_0(q, \phi)$, and therefore the transition frequency Ω are efficiently controlled by two knobs, i.e., by varying the parameters q and ϕ (or, equivalently, Q_0 and Φ)[1)].

The idea underlying the measurement of this charge-flux qubit is based on inducing radio frequency oscillations in the tank circuit of frequency $\omega_{rf} \ll \Omega$ [6]. Due to inductive coupling M, these oscillations cause oscillations of the corresponding flux Φ_T (see Fig. 1*a*) and therefore of the total phase,

$$\phi = \frac{2\pi}{\Phi_0}(\Phi_T + \Phi_m) = \phi_a \sin(\omega_{rf} t + \theta) + \phi_0. \tag{9}$$

If the rf drive signal is sufficiently weak, the amplitude ϕ_a of these oscillations is relatively small, $\phi_a \ll \pi$. In this linear regime, the Josephson inductance is given by

$$L_J^{-1}(n, q, \phi) = \left(\frac{2\pi}{\Phi_0}\right)^2 \frac{\partial^2 E_n(q, \phi)}{\partial\phi^2}. \tag{10}$$

It is therefore determined by the local curvature of the energy surface E_n. For example, for $E_{J0} = 2E_c$ (see

[1)] In fact, the energy spectrum of this system is similar to that of Quantronium [5], having one additional large Josephson junction in the loop.

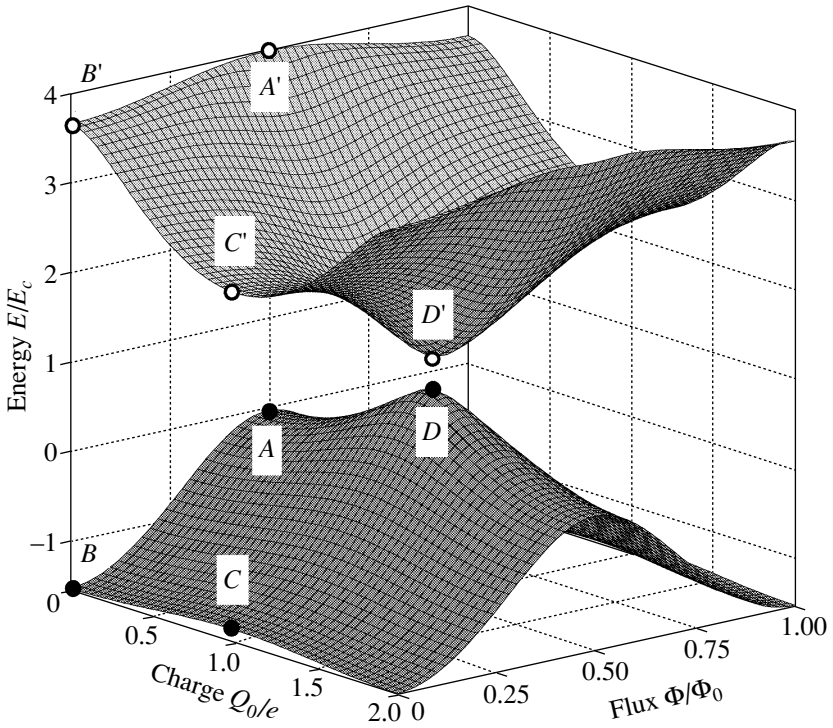

Fig. 2. Shape of the energy bands E_0 and E_1 in the charge-flux qubit calculated for the mean Josephson coupling $E_{J0} \equiv (E_{J1}+E_{J2})/2 = 2E_c$ and the Josephson coupling asymmetry parameter $|j_1 - j_2| = (E_{J1}-E_{J2})/(E_{J1}+E_{J2}) = 0.1$. Black (hollow) circles on the zero (excited) band surface mark the locations of magic points $A\,(A')$, $B\,(B')$, and $C\,(C')$ and the avoided level crossing point $D\,(D')$

Fig. 2) at $q \approx 0$, the respective estimates within the zeroth and first bands are

$$L_J^{-1}(0,0,\phi) \approx 0.4 L_{J0}^{-1} \cos\phi \tag{11}$$

and

$$L_J^{-1}(1,0,\phi) \approx 0.1 L_{J0}^{-1} \cos\phi. \tag{12}$$

In the vicinity of the avoided crossing point, $q = e$ and $\phi = \pi$ (marked as D–D' in Fig. 2), the inverse inductances can increase significantly,

$$L_J^{-1}(n,0,\pi) \approx \frac{(-1)^{n+1}}{4|j_1 - j_2|} L_{J0}^{-1}, \quad n = 0 \text{ and } 1, \tag{13}$$

because of a small asymmetry of the transistor parameters, $|j_1 - j_2| \ll 1$. For example, in the case presented in Fig. 2, $|j_1 - j_2| = 0.1$ and $L_J^{-1} = \mp 2.5 L_{J0}^{-1}$ for the zeroth and first band, respectively. At the points C and C', the absolute values $|L_J^{-1}|$ are smaller but the signs for $n = 0$ and 1 are still different.

Coupling to the qubit causes a shift of the resonance frequency $\omega_0 = (L_T C_T)^{-1/2}$ of the tank circuit, i.e., $\omega_0'(n) = \omega_0 + \delta\omega_0(n)$, where

$$\delta\omega_0(n) = -\frac{1}{2} k^2 \beta_L \frac{L_{J0}}{L_J(n,q,\phi)} \omega_0. \tag{14}$$

Here,

$$k = \frac{M}{\sqrt{L_T L}} < 1 \tag{15}$$

is the dimensionless coupling coefficient. The resonance frequency shift $\delta\omega_0(n)$ carrying information about the qubit state $|n\rangle$ is found from the amplitude or/and phase of forced oscillations in the tank. For achieving sufficient resolution in such measurements, the quality factor of the tank circuit Q should be about or larger than the ratio $\omega_0/|\delta\omega_0(0) - \delta\omega_0(1)|$.

3. INHERENT AND EXTERNAL SOURCES OF DECOHERENCE

In our consideration, we neglected the quasiparticle tunneling that inevitably causes dissipation of energy.

Even rare tunneling of individual quasiparticles across the tunnel junctions, i.e., on and from the island, can decohere the qubit and completely destroy the readout regime described above. These processes lead to a sudden change of the operation point, $q \to q \pm e$ and, possibly, of the energy band index, i.e., cause relaxation $1 \to 0$.

The processes of single quasiparticle tunneling across a small Josephson junction have been studied by Averin and Likharev in Refs. [12, 13]. They generalized the orthodox theory of single electron tunneling to the case of a finite Josephson coupling, $E_J \neq 0$, taking into account the dynamics of the essential phase factors $\exp(\pm i\chi/2)$ in the electron tunneling terms added to the Hamiltonian of type (2). These factors are the operators of a single-electron transfer and their nonzero matrix elements in our basis are

$$e^{\pm}_{nn'} = \langle n, q| \exp(\pm i\chi/2)|q \pm e, n'\rangle. \qquad (16)$$

The rates of transitions $|q, n\rangle \to |q \pm e, n'\rangle$ are given by

$$\Gamma^{\pm}_{nn'} = |e^{\pm}_{nn'}|^2 \frac{I_{qp}(\epsilon^{\pm}_{nn'}/e)}{e} \times \times \left[1 - \exp\left(-\frac{\epsilon^{\pm}_{nn'}}{k_B T}\right)\right]^{-1}. \qquad (17)$$

In our case, $I_{qp}(U)$ is the quasiparticle current–voltage dependence of the network of two tunnel junctions of the qubit connected in parallel. Because the energy surfaces are $2e$-periodic, the corresponding energy gains are identical,

$$\epsilon^{+}_{nn'} = \epsilon^{-}_{nn'} = E_n(q, \phi) - E_{n'}(q \pm e, \phi), \qquad (18)$$

and their value depends on the operation point $\{Q_0, \Phi\}$ (see Fig. 2).

The relation between this energy and the superconductor energy gap Δ_{sc} is important for making the quasiparticle transitions infrequent or even eliminating them. First, if the voltage is $U = \epsilon^{\pm}_{nn'}/e \leq 2\Delta_{sc}/e$, the quasiparticle current $I_{qp}(U)$ entering Eq. (17) is exponentially small, i.e., $\sim I_{c0} \exp(-\Delta_{sc}/k_B T)$[2]. At larger voltages, $U > 2\Delta_{sc}/e$, the current I_{qp} is enormously large, $\geq 2I_{c0}$. Therefore, in order to prevent intensive tunneling of quasiparticles, the energy gain $\epsilon^{\pm}_{nn'}$ must never exceed $2\Delta_{sc}$. Second, if this gain is smaller than Δ_{sc}, then infrequent quasiparticle tunneling can, in principle, be blocked by the gap energy associated with one unpaired electron in the superconducting island (the so-called even–odd parity effect)[3].

Suppression of quasiparticle transitions within the zero energy band in superconducting Al single-charge transistors and Cooper pair boxes was extensively investigated experimentally. Depending on experimental skill and luck (see, e.g., [14–17]), the inspected devices often exhibited pure Cooper pair behavior when their charging energy E_c was not larger than $\sim 100\,\mu$eV $\approx 0.5\Delta_{\rm Al}$, where $\Delta_{\rm Al}$ is the superconductor energy gap of aluminium. Because the energy gain for transitions in the Cooper pair boxes and low-voltage-biased transistors, $\epsilon^{\pm}_{00}$, is less than E_c for any E_J, the condition $E_c < \Delta_{sc}$ can ensure suppression of quasiparticle tunneling in the ground state in a «good» qubit sample.

For quasiparticle transitions from the excited state, this condition is clearly insufficient. For example, for small E_J (corresponding to the flux value $\Phi = \Phi_0/2$, Eq. (3)), the energy gain values are between about E_c (for the process $D' \to A$, see Fig. 2) and $4E_c$ (for the processes $A' \to D'$ and $A' \to D$). At larger E_J, both the minimum and maximum energy gain values are even larger. For example, for $E_J = 4E_c$ (i.e., $\Phi = 0$), the transitions $C' \to B$ and $B' \to C$ correspond to the respective energies $\approx 4E_c$ and $\approx 5E_c$. Because the first factor in the expression for the resulting relaxation rate,

$$[\tau_r^{(\rm qp)}]^{-1} = \Gamma^{+}_{10} + \Gamma^{-}_{10} \approx \approx (|e^{+}_{10}|^2 + |e^{-}_{10}|^2)\frac{I_{qp}(\epsilon^{\pm}_{10}/e)}{e}, \qquad (19)$$

is nonzero for any Q_0 and Φ (see the plots of the two quantities in Fig. 3), only the condition $E_c \leq \Delta_{sc}/5$ can ensure suppression of these transitions at an arbitrary operation point of our qubit. An insufficiently small value of E_c was possibly the reason of a very short relaxation time (tens of ns) in the recent experiment with a charge qubit by Duty et al. [17]. Their Al Cooper pair box had $E_c \approx 0.8\Delta_{sc}$ and $E_J \approx 0.4E_c$, and therefore the energy gain in the chosen operation point ($Q_0 = 0.4e$) was too large, i.e., about $2.2E_c \approx 1.8\Delta_{sc} > \Delta_{sc}$ (although in the ground state, this sample nicely showed the pure Cooper pair characteristic).

Moreover, there are several sources of decoherence due to coupling of the qubit to the environmental degrees of freedom. For evaluating the effect of these

[2] See, for example, a simple approximation formula in S. Ramo, J. R. Whinnery and T. van Duzer, *Fields and Waves in Communication Electronics*, John Wiley and Sons, New York (1965), p. 211.

[3] As follows from the entropy consideration, the threshold value is somewhat smaller than Δ_{sc} for finite volume of island and nonzero temperature, see, for details M. T. Tuominen, J. M. Hergenrother, T. S. Tighe and M. Tinkham, Phys. Rev. Lett. **69**, 1997 (1992).

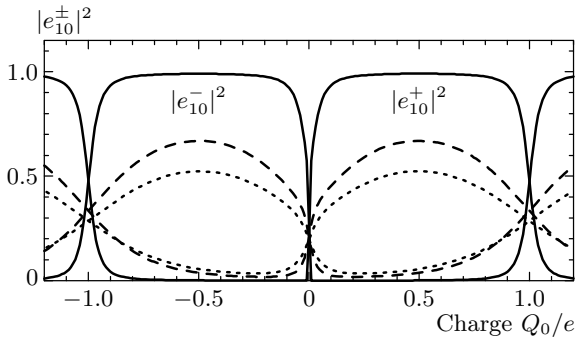

Fig. 3. Off-diagonal matrix elements of the single quasiparticle transfer operators $\exp(\pm i\chi/2)$ computed for different values of the equivalent Josephson coupling set by the flux $\Phi = \Phi_0/2$ (solid lines), $\Phi_0/4$ (dashed lines), and 0 (dotted lines). The qubit parameters are the same as in Fig. 2

sources on the qubit, the coupling Hamiltonian term $H_{coupl} = H_c^{(e)} + H_c^{(m)}$ is included in the total Hamiltonian of the system,

$$H = H_0 + H_{coupl} + H_{bath}, \tag{20}$$

where H_{bath} is a bath operator, and $H_c^{(e)}$ and $H_c^{(m)}$ are the electric control line term and the magnetic coupling term respectively. The latter is associated with both the flux control line and the tank circuit. Fluctuations originating from the sources of gate- and flux-control lines can, in principle, lead to a significant decoherence of the qubit. As was shown in Ref. [18] and demonstrated in experiments [3–5], these effects can, however, be minimized by choosing the appropriate (minimum) coupling. On the other hand, the decoherence caused by the tank-circuit-based readout system requires special analysis, because weakening this coupling results in reducing the input signal. Below, we start with the sources of decoherence associated with the control lines and then analyze the effect of the tank circuit and amplifier.

4. COUPLING TO THE CHARGE CONTROL LINE

The coupling of the charge-phase qubit to the electric control line is actually similar to that of the gate coupling in the ordinary Cooper pair box [18]. However, we here assume that the Josephson coupling parameter λ is not necessarily small, as is usually assumed in the analysis of charge qubits. This generalization of the model is essential because the external flux Φ_m changes the effective Josephson energy (3) of the qubit over a wide range. The assumption that λ is not small implies that the eigenstates of our system, Eq. (5), are generally composed of several (not only two) plane-wave states.

The coupling term can be represented as

$$H_c^{(e)} = -2en\delta V_e, \tag{21}$$

where δV_e is the operator of voltage fluctuations on the island in the absence of the Josephson coupling. The charge operator is equal to $2en = Q_0 - C\hat{V}$, and therefore the essential part of the coupling Hamiltonian is

$$H_c^{(e)} = C\hat{V}\delta V_e. \tag{22}$$

The voltage operator is given by

$$\hat{V} = \frac{\Phi_0}{2\pi}\dot{\varphi} = \frac{\Phi_0}{2\pi}\left(\dot{\chi} - \frac{\partial\gamma}{\partial\phi}\dot{\phi}\right) = \frac{\Phi_0}{2\pi}\dot{\chi}. \tag{23}$$

Here, we assume slow variation of the total phase ϕ, Eq. (9). The voltage operator $\hat{V}$ is similar to the velocity operator of an electron in the periodic electric potential of a crystal lattice [19], and its interband matrix elements are

$$V_{nn'} = \frac{\partial E_n}{\partial q}\delta_{n,n'} + i\frac{E_n - E_{n'}}{2e}\chi_{nn'}(1 - \delta_{n,n'}), \tag{24}$$

where $\delta_{n,n'}$ is the Kroneker delta and $\chi_{nn'}$ are the matrix elements of the phase operator χ [11].

Finally, the coupling Hamiltonian, Eq. (22), takes the form

$$H_c^{(e)} = (\sigma_x \sin\eta_e + \sigma_z \cos\eta_e)X_e, \tag{25}$$

where we introduce the operator

$$X_e = C\|V\|\delta V_e \tag{26}$$

with

$$\|V\| = \frac{1}{2}\sqrt{(V_{11} - V_{00})^2 + 4|V_{01}|^2} \tag{27}$$

and

$$\operatorname{tg}\eta_e = \frac{2|V_{01}|}{(V_{11} - V_{00})}. \tag{28}$$

(The plots of the terms entering Eqs. (27) and (28) obtained by numerical calculations are presented in Fig. 4.) Thus, $X_e = \sum_a C_a x_a$ can be considered as an operator of the bath [20] with the Hamiltonian

$$H_b^{(e)} = \sum_a \left(\frac{p_a^2}{2m_a} + \frac{m_a\omega_a^2 x_a^2}{2}\right) \tag{29}$$

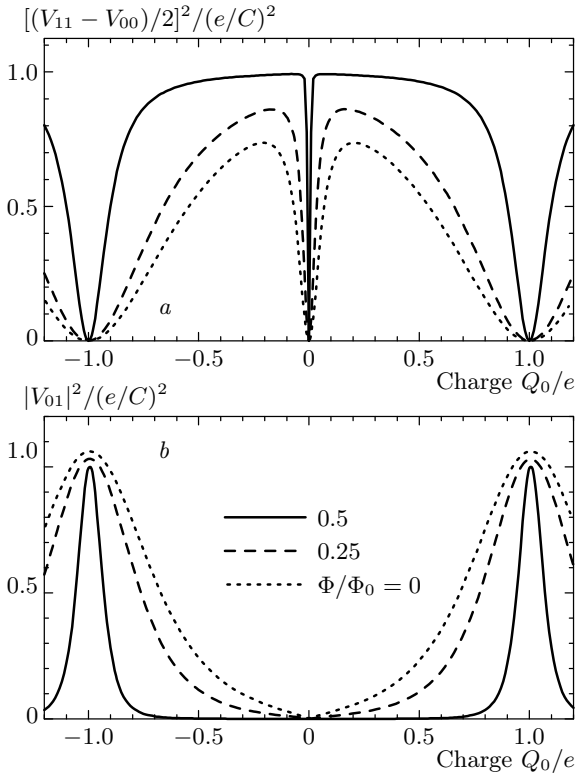

Fig. 4. Terms composed of diagonal (a) and off-diagonal (b) matrix elements of the operator $\hat{V}$ entering Eqs. (27) and (28) are represented for different values of the dimensionless flux Φ_e for the given qubit parameters (see the caption of Fig. 2)

and the spectral density $S_X^{(e)}(\omega) = C^2\|V\|^2 S_V^{(e)}(\omega) = J_e(\omega)\Theta(\omega,T)/\omega$. Here, the oscillator energy function is

$$\Theta(\omega,T) = \frac{\hbar\omega}{2}\operatorname{cth}\frac{\hbar\omega}{2k_BT} \tag{30}$$

and

$$J_e(\omega) = \frac{\pi}{2}\sum_a \frac{C_a^2}{m_a\omega_a}\delta(\omega-\omega_a). \tag{31}$$

With C_g assumed to be small, the spectral density $S_V^{(e)}$ of the fluctuations of δV_e is given by

$$S_V^{(e)}(\omega) = \frac{2}{\pi}\left(\frac{C_g}{C}\right)^2 \operatorname{Re} Z_t(\omega)\,\Theta(\omega,T), \tag{32}$$

where $Z_t = (i\omega C_g + Z_g^{-1})^{-1}$ is determined by the parallel connection of the qubit capacitance $C_gC/(C_g+C) \approx C_g$ and the gate line impedance $Z_g(\omega) \sim R_{100} \equiv 100\,\Omega$. Therefore, for frequencies up to $\omega_g \equiv (R_{100}C_g)^{-1} \gg \epsilon/\hbar$, i.e., at all characteristic frequencies of the system, $\operatorname{Re} Z_t = R_{100}$. This is the case of linear damping in the Caldeira–Leggett model,

$$J_e(\omega) = \frac{\pi}{2}\alpha_e\hbar\omega, \tag{33}$$

with the dimensionless factor

$$\alpha_e(q,\phi) = \left(\frac{C_g\|V\|}{e}\right)^2\frac{R_{100}}{R_Q} \lesssim \left(\frac{C_g}{C}\right)^2\frac{R_{100}}{R_Q}, \tag{34}$$

where $R_Q = h/4e^2 \approx 6.45\,\mathrm{k}\Omega$, the resistance quantum. The estimate similar to the last expression in Eq. (34) was given in Ref. [18] for small λ.

Relaxation and dephasing caused by the charge control line can therefore be described by the spin-boson model with linear damping [21]. The corresponding rates are given by the expressions

$$[\tau_r^{(e)}]^{-1} = \pi\alpha_e \sin^2\eta_e\,\Omega\operatorname{cth}\frac{\hbar\Omega}{2k_BT}, \tag{35}$$

and

$$[\tau_\varphi^{(e)}]^{-1} = [2\tau_r^{(e)}]^{-1} + \pi\alpha_e\cos^2\eta_e\,\frac{2k_BT}{\hbar}. \tag{36}$$

One can see that in accordance with the conclusions in Refs. [18, 22], reducing the coupling coefficient α_e by a small factor $(C_g/C)^2 \ll 1$ can significantly depress the decoherence rates.

5. COUPLING TO THE FLUX CONTROL LINE

The inductive coupling of the qubit loop to the control and readout circuits is described by the Hamiltonian

$$H_c^{(m)} = -\hat{I}_s(\delta\Phi_m + \delta\Phi_T), \tag{37}$$

where $\hat{I}_s$ is the operator of the current circulating in the qubit loop, $\delta\Phi_m = M_m\delta I_m$, the bath operator (proportional to fluctuations of the current δI_m in the control inductance L_m); $\delta\Phi_T = M\delta I$ is the operator of the flux associated with current fluctuations in the tank circuit.

To specify the coupling, we represent the operator $\hat{I}_s$ in the eigenbasis (5), i.e., we find the matrix elements

$$\langle n|\hat{I}_s|n'\rangle, \quad n,n' = 0,\,1. \tag{38}$$

In the general case, $\hat{I}_s$ is given by the expression

$$\hat{I}_s = \kappa_1\dot{Q}_1 + \kappa_2\dot{Q}_2, \tag{39}$$

with the dimensionless factors $\kappa_{1,2} = C_{2,1}/C$ such that $\kappa_1+\kappa_2 = 1$. The quantities

$$Q_{1,2} = -2ei\frac{\partial}{\partial\varphi_{1,2}}$$

are the respective charges on the first and second junction, and their time derivatives are the Josephson supercurrents,

$$\dot{Q}_{1,2} = \frac{i}{\hbar}[Q_{1,2}, H_0] = I_{c1,c2} \sin \varphi_{1,2}. \tag{40}$$

Using the identity

$$\varphi_{1,2} = \frac{\phi}{2} \pm \varphi = \frac{\phi}{2} \pm \chi \mp \gamma$$

and Eq. (4), we can represent the circulating current as

$$\hat{I}_s = I_1(\phi) \cos \chi + I_2(\phi) \sin \chi. \tag{41}$$

The respective amplitudes of these two components are

$$I_1 = \frac{2\pi}{\Phi_0} \frac{E_{J1} E_{J2}}{E_J(\phi)} \sin \phi, \tag{42}$$

and

$$I_2 = (j_1 - j_2)(\kappa_1 j_1 + \kappa_2 j_2) \frac{8\pi}{\Phi_0} \frac{E_{J0}^2}{E_J(\phi)} + \\ + (\kappa_1 - \kappa_2) \frac{4\pi}{\Phi_0} \frac{E_{J1} E_{J2}}{E_J(\phi)} \cos^2 \frac{\phi}{2}. \tag{43}$$

Because the Hamiltonian in Eq. (2) is an even function of χ, the operators $\cos \chi$ and $\sin \chi$ entering Eq. (41) are diagonal and off-diagonal, respectively. The amplitude I_1 is merely the classical Josephson current across two large-capacitance junctions, expressed as a function of the overall phase difference ϕ, while the diagonal term $\cos \chi$ describes the suppression of this current due to the charging effect ($E_c \neq 0$) (see, e.g., Ref. [23]). The second, off-diagonal term in Eq. (41) is due to asymmetry of the transistor; it gives rise to the interband transitions $0 \leftrightarrow 1$. Using the notation

$$c_{00} = \langle 0 | \cos \chi | 0 \rangle, \quad c_{11} = \langle 1 | \cos \chi | 1 \rangle \tag{44}$$

and

$$s_{01} = |\langle 0 | \sin \chi | 1 \rangle|, \tag{45}$$

for the nonzero values of the corresponding matrix elements, we obtain the coupling Hamiltonian in Eq. (37) in the form

$$H_c^{(m)} = (\sigma_y \sin \eta_m + \sigma_z \cos \eta_m)(X_m + X_T), \tag{46}$$

where

$$X_{m,T} = -\|I\| \, \delta\Phi_{m,T}, \tag{47}$$

$$\|I\| = \frac{1}{2} \sqrt{[(c_{11} - c_{00}) I_1]^2 + [2 s_{01} I_2]^2}, \tag{48}$$

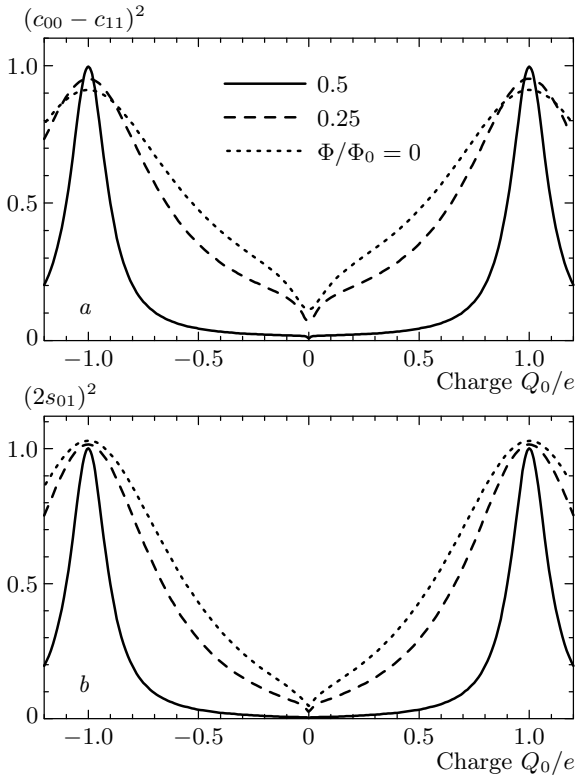

Fig. 5. The terms composed of diagonal (a) and off-diagonal (b) matrix elements of the operator $\cos \chi$ and $\sin \chi$, respectively, calculated for different values of the dimensionless flux Φ_e for the given qubit parameters (see the caption of Fig. 2)

$$\operatorname{tg} \eta_m = \frac{2 s_{01} I_2}{(c_{11} - c_{00}) I_1}, \tag{49}$$

(see the plots of the terms entering these expressions in Fig. 5).

We first omit the term X_T associated with fluctuations of the tank circuit in Eq. (46) and focus on the effect of fluctuations in the flux control line $\delta\Phi_m = M_m \delta I_m$. Assuming real impedance of the flux control line, $Z_m \sim R_{100}$, we obtain the spectral density of the operator $X_m \propto \delta I_m$ in the form $S_X^{(m)}(\omega) = M_m^2 \|I\|^2 S_I^{(m)}(\omega) = J_m(\omega) \Theta(\omega, T)/\omega$. At frequencies below $\omega_m \equiv R_{100}/L_m$, the function J_m is linear,

$$J_m(\omega) = \frac{\pi}{2} \alpha_m \hbar \omega \tag{50}$$

with the dimensionless coupling factor

$$\alpha_m(q, \phi) = \left(\frac{2 M_m \|I\|}{\Phi_0} \right)^2 \frac{R_Q}{R_{100}}. \tag{51}$$

At higher frequencies, $\omega > \omega_m$, the effective damping decays as $(\omega_m/\omega)^2$.

In fact, Eq. (51) describes the effect of coupling to the control flux in the general case. An estimate of the coupling factor based on the evaluation

$$\|I\| \approx \frac{1}{2}\left|\frac{\partial E_J}{\partial \Phi}\right|, \tag{52}$$

which is valid for a symmetric transistor ($I_2 = 0$) with small E_J, was made in [18]. Small mutual inductance M_m [18, 22] leads to small α_m and therefore causes significant depression of the corresponding relaxation rate,

$$[\tau_r^{(m)}]^{-1} = \pi\alpha_m \sin^2\eta_m\, \Omega \operatorname{cth}\frac{\hbar\Omega}{2k_BT}, \tag{53}$$

and dephasing rate,

$$[\tau_\phi^{(m)}]^{-1} = [2\tau_r^{(m)}]^{-1} + \pi\alpha_m \cos^2\eta_m\, \frac{2k_BT}{\hbar}. \tag{54}$$

So far, we have considered the effects of decoherence due to the charge and flux control lines as two independent effects. They must actually be described together using a multibath model [18]. If either of these decoherence effects is small, i.e., the so-called Hamiltonian-dominated regime is realized, the total rates due to contributions of the two control lines are given by

$$[\tau_r^{(c)}]^{-1} = [\tau_r^{(e)}]^{-1} + [\tau_r^{(m)}]^{-1}, \tag{55}$$

$$[\tau_\varphi^{(c)}]^{-1} = [2\tau_r^{(c)}]^{-1} + [\tau_\varphi^{(e)}]^{-1} + [\tau_\varphi^{(m)}]^{-1}. \tag{56}$$

In our model, we assume that such a regime is realized and, moreover, the resulting rates in Eqs. (55) and (56) can be made negligibly small. Below, we focus on the effect of the readout circuit, whose coupling strength has to be optimized.

6. DECOHERENCE DUE TO THE READOUT SYSTEM

In contrast to control lines, coupling to a readout device (in our case, the tank circuit with an amplifier) cannot be made arbitrarily small in order to reduce the decoherence. This coupling should ensure sufficiently strong signals at the amplifier input in order to perform a measurement with a reasonable signal-to-noise ratio on a time scale shorter than that determined by other factors, namely $\tau_r^{(c)}$. Moreover, without an efficient switch (see a possible design of such a switch, e.g., in Ref. [24]), such a coupling may cause significant dephasing of the qubit during quantum gate manipulation.

The inductive qubit coupling to the tank circuit is described by the Hamiltonian in Eq. (46). The spectral density of fluctuations of the corresponding variable $X_T \propto \delta\Phi_T = M\delta I$ is expressed as

$$S_X^{(T)}(\omega) = \frac{2}{\pi}M^2\|I\|^2 S_I^{(T)}(\omega) = J_T(\omega)\frac{\Theta(\omega, T^*)}{\omega}, \tag{57}$$

where $S_I^{(T)}(\omega)$ is the spectral density of the noise current δI across the inductance L_T. Because the cold (superconducting) tank circuit itself presumably has very low losses, a back-action noise δI of the amplifier is dominating. It is associated with the input real impedance, modeled by R_p or R_s for parallel and serial configurations, respectively (see Fig. 1). T^* is the effective temperature associated with this impedance.

The spectral density $S_I^{(T)}$ and the function $J_T(\omega)$ can be found from a network consideration. With the small detuning $\delta\omega_0 \ll \omega_0$ neglected, in the case of the parallel network (Fig. 1*b*), the spectral function J_T is given by the expression

$$J_T^{(p)}(\omega) = \frac{2}{\pi}\alpha_p\hbar\omega\frac{\omega_0^4}{(\omega^2-\omega_0^2)^2 + \omega^2\omega_0^2Q^{-2}}, \tag{58}$$

with

$$\alpha_p = \left(\frac{2M\|I\|}{\Phi_0}\right)^2\frac{R_Q}{R_p} = \frac{k^2\beta_L}{\pi Q}\,\frac{\|I\|^2}{e\omega_0 I_{c0}} \tag{59}$$

and with the quality factor $Q = \omega_0 C_T R_p = R_p/\omega_0 L_T$. For the serial network shown in Fig. 1*c*, we have

$$J_T^{(s)}(\omega) = \frac{2}{\pi}\alpha_s\hbar\omega\frac{\omega^2\omega_0^2}{(\omega^2-\omega_0^2)^2 + \omega^2\omega_0^2Q^{-2}}, \tag{60}$$

with

$$\alpha_s = \left(\frac{2M\|I\|}{\Phi_0}\right)^2\frac{R_QR_s}{(\omega_0 L)^2} \tag{61}$$

and $Q = (\omega_0 C_T R_s)^{-1} = \omega_0 L_T/R_s$.

In contrast to the linear spectral functions for the control lines, Eqs. (33) and (50), the functions given by Eqs. (58) and (60) describe a structured bath, i.e., they both are of a Lorentzian (resonance) shape. A similar situation emerges, for example, in the case of the flux qubit with readout using a C-shunted dc SQUID [22]. The spin-boson model with a structured bath was analyzed theoretically in [25] on the basis of the flow equations. If the coupling is weak, as in our case, only the high frequency ($\omega \sim \Omega$) and low frequency ($\omega \to 0$) behaviors of $J(\omega)$ account for relaxation and dephasing, respectively [22, 26, 27].

Because the frequency Ω is typically about tens of GHz and the distance between the qubit and the amplifier presumably exceeds the wavelength, the effective

real admittance of the parallel circuit at these frequencies is equal to R_{100}^{-1} and the impedance of the serial circuit is $\approx R_{100}$. Therefore, the relaxation rates increase by the respective factors $g_p = R_p/R_{100} \gg 1$ and $g_s = R_{100}/R_s \gg 1$.

For the parallel tank circuit, the relaxation and dephasing rates (presumably, $\ll \omega_0$) are equal to

$$[\tau_r^{(p)}]^{-1} = \pi g_p \alpha_p \sin^2 \eta_m \left(\frac{\omega_0}{\Omega}\right)^4 \Omega \operatorname{cth} \frac{\hbar\Omega}{2k_B T^*}, \quad (62)$$

and

$$[\tau_\varphi^{(p)}]^{-1} = [2\tau_r^{(p)}]^{-1} + \pi \alpha_p \cos^2 \eta_m \frac{2k_B T^*}{\hbar}, \quad (63)$$

respectively. The relaxation rate is dramatically suppressed due to the small frequency ratio, $(\omega_0/\Omega) \ll 1$. For the serial configuration, the corresponding rates are

$$[\tau_r^{(s)}]^{-1} = \pi g_s \alpha_s \sin^2 \eta_m \left(\frac{\omega_0}{\Omega}\right)^2 \Omega \operatorname{cth} \frac{\hbar\Omega}{2k_B T^*}, \quad (64)$$

$$[\tau_\varphi^{(s)}]^{-1} = [2\tau_r^{(s)}]^{-1}. \quad (65)$$

The dephasing rate is determined by the rate of relaxation, because at low frequency, $\omega \ll \omega_0$, the function $J_T^{(s)}(\omega) \propto \omega^3$ [21]. Due to weaker decay of the serial circuit impedance at high frequencies, $\omega \gg \omega_0$, the relaxation rate is, however, substantially higher than in the case of the parallel circuit configuration. We therefore focus our further consideration only on the parallel tank circuit as the more favorable (allowing longer measuring time).

7. MAGIC POINTS AND SOME ESTIMATIONS

The analysis of the coupling between the qubit and the tank circuit, Eqs. (46)–(49) and Fig. 5, shows that its strength $X_T \propto \|I\|$ and mixing angle η_m can be significantly varied by choosing an appropriate operation point. For example, as can be seen from Eq. (42), the diagonal component of X_T ($\propto I_1$), which essentially causes pure dephasing of the qubit, is zero, i.e., the mixing angle $\eta_m = \pi/2$, at the phase values $\phi = 0$ and π. The derivatives $\partial E_{0,1}/\partial\phi$ and therefore the circulating supercurrent are zero. Moreover, as illustrated in Fig. 5*b*, if the gate charge $Q_0 \approx 0$ (i.e., derivatives $\partial E_{0,1}/\partial Q_0 = 0$), then $|s_{01}|$ and hence X_T are minimum. In particular, at the bias flux $\Phi_m = \Phi_0/2$ or, equivalently, $\phi = \pi$ (this point is marked as A in Fig. 2), $E_J(\phi) = |E_{J1} - E_{J2}| \ll E_c$, and we can therefore use the explicit expressions for the wave functions, Eqs. (A.11) and (A.12) in Ref. [11], and obtain

$$|s_{01}| = \frac{1}{16\sqrt{2}} \frac{E_J(\phi)}{E_c} = \frac{|j_1 - j_2|}{8\sqrt{2}} \frac{E_{J0}}{E_c}. \quad (66)$$

Then the value of $\|I\|$ given by (48) is

$$\|I\|_A = 2|s_{01}|I_2 \approx \frac{|j_1 - j_2|}{8\sqrt{2}} \frac{E_{J0}}{E_c} I_{c0}, \quad (67)$$

where we have taken into account that $\kappa_1 \sim \kappa_2 \sim 0.5$ and the second term in Eq. (43), $\propto (\kappa_1 - \kappa_2)$, vanishes because $\cos(\phi/2) = 0$. At the point $Q_0 = 0, \phi = 0$ (marked as B in Fig. 2), the Josephson energy $E_J(\phi) = 2E_{J0}$ and $2|s_{01}|$ is approximately equal to $(1/8\sqrt{2})E_{J0}/E_c$, and therefore

$$\|I\|_B \approx \frac{|j_1 - j_2 + \kappa_1 - \kappa_2|}{8\sqrt{2}} \frac{E_{J0}}{E_c} I_{c0}, \quad (68)$$

while for $Q_0 = e$ (point C in Fig. 2), $|s_{01}| \approx 0.5$ and

$$\|I\|_C \approx |j_1 - j_2 + \kappa_1 - \kappa_2| I_{c0}. \quad (69)$$

It is remarkable that the effect of asymmetry in critical currents and capacitances of the junctions can, in principle, cancel if $(j_1 - j_2) = -(\kappa_1 - \kappa_2)$. In practice, however, the signs of $(j_1 - j_2)$ and $(\kappa_1 - \kappa_2)$ are normally similar because the critical current and capacitance are both proportional to the junction area and such cancelling does not occur.

Comparing Eqs. (67), (68), and (69), we can see that under the assumption of small asymmetry of the transistor, $j_1 \approx j_2 \approx \kappa_1 \approx \kappa_2 \approx 0.5$, the coupling strength α_p at the points A ($Q_0 = 0$, $\phi = \pi$), B ($Q_0 = 0$, $\phi = 0$), and C ($Q_0 = e$, $\phi = 0$) is rather small, but it is significant at the point D ($Q_0 = e$, $\phi = \pi$), where the parameter $|s_{01}| \approx 0.5$ and

$$\|I\|_D \approx I_{c0}. \quad (70)$$

To illustrate this behavior, the coupling strength evaluated for typical parameters of the system is presented in the Table.

From the standpoint of operation with a minimum dephasing rate, the «magic» points A, B, and C at which the supercurrent $I_1 = 0$ (see Eq. (42)) are clearly preferable to other points in the Q_0–Φ plane. Therefore, manipulation of the qubit can, in principle, be performed at any of these points. The estimated values of the corresponding fidelity factor for quantum manipulation, $Q_\varphi \equiv \Omega\tau_\varphi^{(p)}$, given in the Table, are sufficiently high. For example, in the case of preparation of the qubit at point A, the manipulation can be performed by means of a dc pulse applied to the transistor gate [3, 4, 17]. This pulse (with short rise and fall times) can rapidly switch the qubit, for example, to point D and back to A causing its evolution (although with significant dephasing) during the pulse span. Our qubit

Evaluated qubit parameters derived under the assumption that $E_{J0} = 2E_c = 80\,\mu$eV (i.e., $I_{c0} \approx 40$ nA and $5E_c = \Delta_{\rm Al} \approx 200\,\mu$eV, the energy gap of Al) and $j_1 - j_2 = \kappa_1 - \kappa_2 = 0.1$. The tank circuit quality factor $Q = 100$, frequency $\omega_0 = 2\pi \cdot 100$ MHz, $(L_T/C_T)^{1/2} = 100\,\Omega$, $k^2 Q\beta_L = 20$ and temperature $T^* = 1\,\text{K} \gg T \sim 20$ mK. As long as the dephasing rate at the magic points is nominally zero, a 0.1% inaccuracy of the adjustment of the values $\phi = \pi$ and 0 was assumed

Operation point:	A–A'	B–B'	C–C'	D–D'
Frequency $\Omega/2\pi$, GHz	39	50	36	4
Coupling strength α_p	$2 \cdot 10^{-2}$	10^{-2}	$4 \cdot 10^{-2}$	1
Qubit fidelity factor Q_φ	$3 \cdot 10^4$	$2 \cdot 10^5$	10^4	< 30
Relaxation time $\tau_r^{(p)}$, s	$8 \cdot 10^{-2}$	10^{-1}	$6 \cdot 10^{-3}$	10^{-7}

prepared in the ground state at point A or B or C can be (preferably) manipulated by a pulse of microwave frequency, $\sim \Omega$, applied to the gate. For example, the Quantronium qubit in the experiment by Vion et al. [5] was manipulated by microwave pulses at point C.

For reading out the final state, the qubit dephasing is of minor importance, while the requirement of a sufficiently long relaxation time is decisive. Moreover, the relaxation rate may somewhat increase due to oscillations in the tank induced by a drive pulse (see Fig. 6), which leads to the development of oscillations around a magic point along the ϕ axis, Eq. (9). If the frequency of these oscillations is sufficiently low, $\omega_{rf} \ll \Omega$, they result only in a slow modulation of the transition frequency Ω. The increase of the amplitude of steady oscillations up to $\phi_a \approx \pi/2$ (determined by the amplitude of the drive pulse and detuning) yields a large output signal and still ensures the required resolution in the measurement provided the product $k^2 Q\beta_L > 1$ is sufficiently large. (At larger amplitudes ϕ_a, the circuit operates in a nonlinear regime probing the averaged reverse inductance of the qubit whose value, as well as the produced frequency shift $\delta\omega_0$, is smaller [28].) Because points A and B lie on the axis $Q_0 = 0$ and are both characterized by a sufficiently long relaxation time, reading-out of the qubit state with the rf oscillation span $\pm\pi/2$ is preferable at either point. In the case of operation point C, the limited amplitude of the oscillations does not significantly reduce the relaxation time either. Significant reduction of the relaxation time occurs in the vicinity of point D. Because of this property, which is due to the dependence of the transversal coupling strength on ϕ, Eqs. (43)–(49), the measurement of the Quantronium state using a switching current technique was possible in the middle of segment CD (see Fig. 2), where the maximum values of the circulating current in the excited and ground states were of different signs [5].

In the vicinity of level crossing point D, in which the gap between the zeroth and the first excited states is minimum, $\hbar\Omega = 2|j_1 - j_2|E_{J0}$, oscillations of ϕ may cause the Landau–Zener transitions $|0\rangle \leftrightarrow |1\rangle$ [29]. The probability of a such transition per single sweep,

$$p_{\rm LZ} = \exp\left[-2\pi \frac{(j_1 - j_2)^2 E_{J0}}{\phi_a \hbar\omega_{rf}}\right], \qquad (71)$$

can be appreciable in a sufficiently symmetric transistor and/or at a high driving frequency ω_{rf}, i.e., when $|j_1 - j_2| \lesssim (\hbar\omega_{rf}/E_{J0})^{1/2}$. These transitions lead to unwanted mixing of the qubit states [30]. In the vicinity of point A', where the gap between the first and the second (not shown in Fig. 2) energy bands is smaller [9], $\hbar\Omega_{12} = (j_1 - j_2)^2 E_{J0}^2/2E_c$, the Landau–Zener transitions $|1\rangle \leftrightarrow |2\rangle$ are more probable. Fortunately, the second energy band has a positive curvature, $\partial^2 E_2(0, \phi = \pi)/\partial\phi^2 > 0$, and therefore the mixing of these states might even improve the distinguishability of signals from the ground and excited states. More rigorous analysis of this effect on operation of the qubit at point A is needed, however.

We finally evaluate the time of measurement required for the resolution of the states $n = 0$ and $n = 1$ at the most favorable magic points A and B. As schematically shown in Fig. 6, an rf drive pulse is applied to the tank circuit just after manipulation of the qubit ($t = 0$) and induces growing oscillations in the tank. The amplitude of the oscillations of voltage V approaches a steady value A_0 (A_1) for $n = 0$ ($n = 1$) after the time $t_{rise} \approx 2\pi Q/\omega_0$. Assuming a corresponding amplitude of oscillations of the phase $\phi_a = \pi/2$, we obtain the amplitudes

$$A_0 = \phi_a \frac{\Phi_0}{2\pi} \frac{\omega L_T}{M} = \left(\frac{\pi\Phi_0 \omega R_p I_{c0}}{8k^2 Q\beta_L}\right)^{1/2} \approx 3\,\mu\text{V} \qquad (72)$$

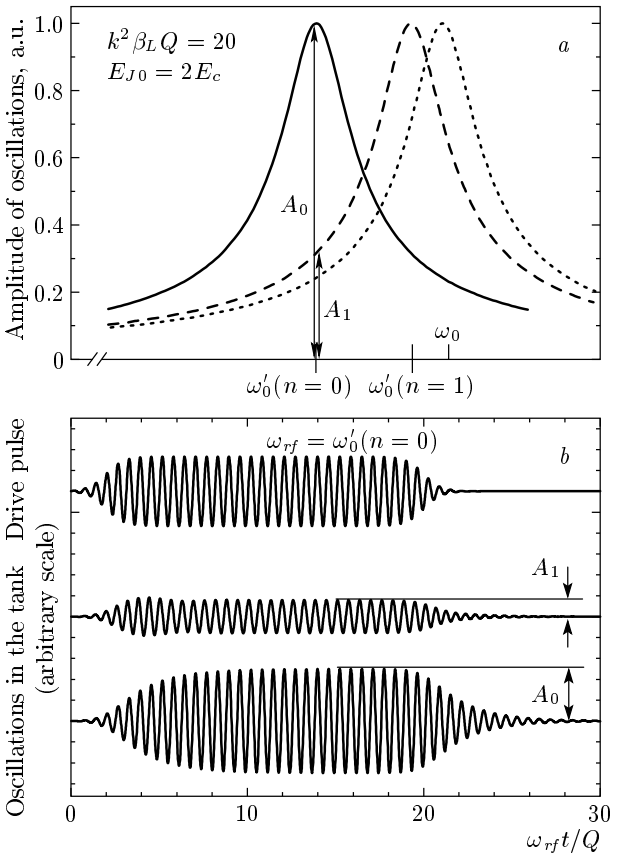

Fig. 6. The principle of narrow-band radio-frequency readout of the qubit. (a) The resonance curves of the uncoupled tank circuit (dotted line) and the tank circuit coupled to the qubit biased at operation point A in the excited state (dashed line) and in the ground state (solid line). (b) Driving pulse applied to the tank circuit (top curve) and the response signal of the tank in resonance (the ground qubit state, bottom curve) and outside resonance (excited state, middle curve). A smooth envelope of the driving pulse is used to suppress transient oscillations and has a small effect on the rise time of the response signal. For clarity, the curves are shifted vertically

and $A_1 \approx 1\,\mu$V for the parameters in the Table.

Assuming that the equivalent noise of a semiconductor-based amplifier referred to the input is of the order of the Johnson voltage noise across $R_p \approx 10\,\mathrm{k}\Omega$ at ambient temperature $T^* \sim 2\,$K, i.e., $S_V^{1/2} \approx 1\,\mathrm{nV}/\sqrt{\mathrm{Hz}}$, we can express the signal-to-noise ratio as

$$\mathrm{SNR} = \frac{(A_0 - A_1)\sqrt{t_{meas}}}{S_V^{1/2}} \approx 2 \cdot 10^3 \sqrt{t_{meas}/1\,\mathrm{s}}, \quad (73)$$

where t_{meas} is the time of measurement. This time should clearly be much shorter than the relaxation time $\tau_r^{(p)}$ (evaluated as $\approx 0.1\,$s, see the Table) and exceed the rise time of the oscillations in the tank $t_{rise} \approx 1\,\mu$s (the latter condition nicely agrees with the requirement $\mathrm{SNR} > 1$). Thus, a drive pulse duration of $\sim 10\,\mu$s ensuring $t_{meas} \sim 10\,\mu$s seems to be a good choice because it yields the sufficiently high value of $\mathrm{SNR} \approx 6$. The latter (as well as the quantum fidelity factor Q_φ) can be substantially improved using a SQUID-based low-noise amplifier [31].

8. CONCLUSION

We have demonstrated that both manipulation and readout of the charge-phase qubit coupled to a tank circuit is, in principle, possible. More specifically, the decoherence effect of the electric and magnetic control lines can seemingly be minimized by reducing coupling to the qubit. The readout system based on the parallel tank circuit and cold amplifier can ensure sufficiently weak dephasing in the regime without an rf drive. The dephasing rate strongly depends on the accuracy of adjusting the offset flux bias $\Phi_m = 0$ or $\Phi_m = \Phi_0/2$ corresponding to operation at the magic points. High symmetry of the Josephson junction parameters may further improve the coherence characteristics of the qubit. Because the LC resonance tank circuit introduces only small noise at the high transition frequency of the qubit, $\Omega \gg \omega_0$, the rate of relaxation can also be made sufficiently small. Applying an rf drive pulse of limited span allows a readout of the qubit state in the regimes of single and repeated measurements.

Other problems in engineering Josephson qubits with weak decoherence are the $1/f$ noise of critical currents of Josephson junctions [32] and the $1/f$ background noise coupled to the charge variable [33], which have not been addressed in this paper but are equally important. Hopefully, in the given system, these effects might not be as strong as in «traditional» tunnel-junction devices like dc SQUIDs and single-electron transistors operating at nonzero voltage bias. Due to perfect decoupling of the superconducting loop with the single-charge transistor from dc bias lines and due to the coherent nature of the Josephson current in the zero voltage bias regime, one could expect a minor back-action effect of the zero-bias operating transistor on its critical current noise and charge noise, which dramatically depend on the current fed (see, for example, Ref. [34]).

The author would like to thank Per Delsing, Yuriy

Makhlin, and Frank Wilhelm for stimulating discussions. This work was partially supported by the European Union through the SQUBIT-2 project.

REFERENCES

1. J. Clarke, Science **299**, 1850 (2003) and references therein.
2. V. Bouchiat, D. Vion, P. Joyez, D. Esteve, and M. Devoret, Phys. Scripta **T76**, 165 (1998).
3. Y. Nakamura, Yu. A. Pashkin, and J. S. Tsai, Nature **398**, 768 (1999); Yu. A. Pashkin, T. Yamamoto, O. Astafiev, Y. Nakamura, D. V. Averin, and J. S. Tsai, Nature **421**, 823 (2003).
4. K. Bladh, D. Gunnarson, G. Johansson, A. Käck, G. Wendin, A. Aassime, M. Taslakov, and P. Delsing, Phys. Scripta **T102**, 167 (2002).
5. D. Vion, A. Aassime, A. Cottet, P. Joyez, H. Pothier, C. Urbina, D. Esteve, and M. H. Devoret, Science **296**, 886 (2002).
6. A. B. Zorin, Physica C **368**, 284 (2002).
7. R. Rifkin and B. S. Deaver, Jr., Phys. Rev. B **13**, 3894 (1976).
8. D. V. Averin, Phys. Rev. Lett. **88**, 207901 (2002).
9. *Handbook of Mathematical Functions*, ed. by M. Abramowitz and I. A. Stegun, U.S. GPO, Washingtin, D.C. (1972), Chapter 20.
10. D. V. Averin, A. B. Zorin, and K. K. Likharev, Zh. Eksp. Teor. Fiz. **88**, 697 (1985).
11. K. K. Likharev and A. B. Zorin, J. Low Temp. Phys. **59**, 347 (1985).
12. D. V. Averin, Fiz. Nizk. Temp. **13**, 364 (1987) [Sov. J. Low Temp. **13**, 208 (1987)].
13. D. V. Averin and K. K. Likharev, in *Mesoscopic Phenomena in Solids*, ed. by B. L. Altshuler, P. A. Lee, and R. A. Webb, Elsevier, Amsterdam (1991), p. 175.
14. P. Joyez, P. Lafarge, A. Filipe, D. Esteve, C. Urbina, and M. H. Devoret, Phys. Rev. Lett. **72**, 2458 (1994).
15. A. Amar, D. Song, C. J. Lobb, and F. C. Wellstood, Phys. Rev. Lett. **72**, 3234 (1994).
16. J. Männik and J. E. Lukens, Phys. Rev. Lett. **92**, 057004 (2004).
17. T. Duty, D. Gunnarsson, K. Bladh, R. J. Schoelkopf, and P. Delsing, E-print archives, cond-mat/0305433.
18. Yu. Makhlin, G. Schön, and A. Shnirman, Rev. Mod. Phys. **73**, 357 (2001).
19. E. M. Lifshitz and L. P. Pitaevskii, *Statistical Physics*, Part 2, Pergamon Press, Oxford (1980).
20. A. O. Cladeira and A. J. Leggett, Ann. Phys. **149**, 374 (1983).
21. A. J. Leggett, S. Chakravarty, A. T. Dorsey, M. P. A. Fisher, A. Garg, and W. Zwerger, Rev. Mod. Phys. **59**, 1 (1987).
22. C. H. van der Wal, F. K. Wilhelm, C. J. P. M. Harmans, and J. E. Mooij, Eur. Phys. J. B **31**, 111 (2003).
23. A. B. Zorin, Phys. Rev. Lett. **76**, 4408 (1996).
24. J. Clarke, T. L. Robertson, B. L. T. Plourde, A. García-Martinez, P. A. Reichardt, D. J. van Harlingen, B. Chesca, R. Kleiner, Y. Makhlin, G. Schön, A. Shnirman, and F. K. Wilhelm, Phys. Scripta **T102**, 173 (2002).
25. S. Kleff, S. Kehrein, and J. von Delft, E-print archives, cond-mat/0304177.
26. M. Grifoni, E. Paladino, and U. Weiss, Eur. Phys. J. B **10**, 719 (1999).
27. L. Tian, S. Lloyd, and T. P. Orlando, Phys. Rev. B **65**, 144516 (2002).
28. A. B. Zorin, Phys. Rev. Lett. **86**, 3388 (2001).
29. L. D. Landau, Phys. Z. Sowjetunion **1**, 89 (1932); C. Zener, Proc. R. Soc. London, Ser. A **137**, 696 (1932).
30. A. V. Shytov, D. A. Ivanov, and M. V. Feigel'man, E-print archives, cond-mat/0110490.
31. M.-O. André, M. Mück, J. Clarke, J. Gail, and C. Heiden, Appl. Phys. Lett. **75**, 698 (1999).
32. D. J. van Harlingen, Talk at NATO Advanced Research Workshop *Coherent Charge and Spin Transport on a Nanoscale* (June 8–12, 2003, Chernogolovka, Moscow Region, Russia), E-print archives, http://www.itp.ac.ru/∼meso03/pdf/van_harlingen.pdf.
33. E. Paladino, L. Faoro, G. Falci, and R. Fazio, Phys. Rev. Lett. **88**, 228304 (2002).
34. V. A. Krupenin, D. E. Presnov, M. N. Savvateev, H. Scherer, A. B. Zorin, and J. Niemeyer, J. Appl. Phys. **84**, 3212 (1998).